

Aerodynamic behaviour of double hinged articulated loading platforms

Mohd Moonis Zaheer¹, Syed Danish Hasan^{*1}, Nazrul Islam² and Moazzam Aslam³

¹Department of Civil Engineering, Z.H. College of Engg. & Tech., AMU, Aligarh, India

²Department of Civil Engineering, Jamia Millia Islamia, New Delhi-110025, India

³Civil Engineering Section, University Polytechnic, AMU, Aligarh, India

(Received November 17, 2020, Revised February 24, 2021, Accepted February 27, 2021)

Abstract. Articulated loading platforms (ALPs) belongs to a class of offshore structures known as compliant. ALP motions have time periods falling in the wind excitation frequency range due to their compliant behaviour. This paper deals with the dynamic behavior of a double hinged ALP subjected to low-frequency wind forces with random waves. Nonlinear effects due to variable submergence, fluctuating buoyancy, variable added mass, and hydrodynamic forces are considered in the analysis. The random sea state is characterized by the Pierson-Moskowitz (P-M) spectrum. The wave forces on the submerged elements of the platform's shaft are calculated using Morison's Equation with Airy's linear wave theory ignoring diffraction effects. The fluctuating wind load has been estimated using Ochi and Shin wind velocity spectrum for offshore structures. The nonlinear dynamic equation of motion is solved in the time domain by the Wilson- θ method. The wind-structure interactions, along with the effect of various other parameters on the platform response, are investigated. The effect of offset of aerodynamic center (A.C.) with the center of gravity (C.G.) of platform superstructure has also been investigated. The outcome of the analyses indicates that low-frequency wind forces affect the response of ALP to a large extent, which otherwise is not enhanced in the presence of only waves. The mean wind modifies the mean position of the platform surge response to the positive side, causing an offset. Various power spectral densities (PSDs) under high and moderate sea states show that apart from the significant peak occurring at the two natural frequencies, other prominent peaks also appear at very low frequencies showing the influence of wind on the response.

Keywords: aerodynamic effects; wave forces; articulated loading platform; wind-induced response

1. Introduction

Although wave loading on offshore platforms is generally assumed to be more significant than wind loading, exceptions can be found. Low frequency articulated loading platforms (ALPs) reduce the response to high-frequency wave forces. However, the structure vibrates within the range of the

*Corresponding author, Associate Professor, E-mail: sdhasan.amu@gmail.com

^a Associate Professor, E-mail: mooniszaheer@rediffmail.com

^b Professor, E-mail: nazrulislam.jmi@gmail.com

^c Assistant Professor, E-mail: moazzam_aslam22@rediffmail.com

most energetic low frequencies of wind excitation, as shown in Fig. 1. This indicates the crucial impact of wind action on the behavior of ALPs.

The articulated loading platforms, due to their compliant nature, are more susceptible to the dynamic wind loads than are the conventional fixed platforms. The presence of wind, waves, and currents cause the platforms to have mean and fluctuating effects in the direction of loading. The primary effects of waves, which have dominant frequencies higher than those of wind, are not very significant to the overall motion of ALPs. However, low-frequency wind forces may result in the low-frequency resonant oscillations of ALPs. These oscillations in surge are typically four to five times the wave frequency oscillations (Kareem 1985).

The wind-induced vibration of ALPs is a complicated phenomenon due to fluid-structure interaction effects. There is a lack of a comprehensive study conducted to investigate the wind-induced vibration of such platforms. Some studies related to these vibrations are available on other compliant platforms such as TLPs, Spar, FPSO, guyed towers, and offshore wind turbines (Abou-ryan *et al.* 2016, Bae and Kim 2011, Islam *et al.* 2014, Karimirad and Moan 2012, Kim and Kim 2015, Moharrami and Tootkaboni 2014, Oyejobi *et al.* 2016, Rahman *et al.* 2017, Ye and Ji 2019). Chandrasekaran *et al.* (2013) developed a mathematical model for analyzing triceratops, a new generation offshore platform, under wind loads. The nonlinear response of stiffened triceratops under impact and non-impact waves was studied by Chandrasekaran and Nassery (2017). In a recent study, offshore triceratops' analysis in ultra-deep waters under the combined action of wind, wave, and current forces was performed by Nagavinothini and Chandrasekaran (2019). It showed response enhancement with the increase in significant wave height and wind velocity.

The dynamic behaviour of TLP supporting a wind turbine under multi-directional waves was investigated by Abou-ryan *et al.* (2016). Diffraction and Froude-Krylov wave forces of TLP for surge, sway and heave motions under different wave periods and three-wave approach angles have been investigated by Malayjerdi and Tabeshpour (2016) and found that diffraction force for heave in low wave periods are dominant. Ahmad *et al.* (1997) conducted dynamic analysis on a TLP. They found that the magnitude of the wind force and the location of the aerodynamic center (A.C.) significantly influence the surge and yaw responses of TLP. In another study, Jain and Chandrasekaran (2004) investigated the effect of wind and wave forces on the behavior of a triangular TLP. The effect of offset of A.C. and C.G. of the platform on the coupled response of triangular TLP was also investigated. The outcome shows that geometric properties of the platform, like locations of aerodynamic center (A.C.) and center of gravity (C.G.) play a vital role in the overall dynamic response of the platform. El-gamal *et al.* (2014) studied the tension force effect of tethers on the response of a square TLP under ocean waves and found that surge response decreases as tether tension force increases. Santo *et al.* (2015) presented a new mathematical approach for determining hydrodynamic loads on a compliant tower subjected to the combined action of waves and current and showed that reduction of force on such platforms due to the current blockage effect is genuine and substantial. However, this study is limited to regular waves. Zaheer and Islam (2008) conducted an extensive state-of-the-art review of the aerodynamic behaviour of articulated towers. In another study by the same authors, Zaheer and Islam (2017) compared the response of a double hinged articulated tower under wave alone and combined wind and waves. The response of multi-hinged articulated offshore tower under vertical ground excitation was studied by Hasan *et al.* (2011). For exploring oil and gas in deep-sea conditions, marine risers' strengthening by fiber-reinforced polymer (FRP) for improved durability and its dynamic characteristics was examined by Islam (2018). The efficiency of articulated joints and control of platform response when deployed in ALPs, processing platforms, and multi-legged articulated towers are presented in various published

literature (Chandrasekaran *et al.* 2010, Islam *et al.* 2009a,b Zaheer and Islam 2010; Philip *et al.* 2015).

The published literature lacks the dynamic analysis of double hinged ALP under a random ocean environment. Hence, it is vital to perform dynamic analysis of ALP under the combined wind, wave, and current forces. Further, the effect of offset of aerodynamic center (A.C.) and center of gravity (C.G.) on the dynamic response of ALP did not find any reporting in the published work, making the present study novel. Therefore, the present study is carried out with the following objectives:

1. To perform a random vibration analysis of ALP in the time domain using the simulation procedure for wind, waves, and currents.
2. To study the effect of offset of A.C. with respect to C.G. on the platform response.

2. Mathematical modeling and analysis

2.1 Modeling of ALP

In the present study, an ALP is modeled as a rigid body enacted by two articulated joints, as shown in Fig. 2. The in-plane rotations at the two articulated joints constitute the dynamic degree-of-freedom of the system. Fig. 3 (a) and 3(b) show the plan and superstructure details of the platform deck taken for the present study. The platform structure is idealized by replacing its mass distribution with discrete masses located at the centroids of a series of small elements of length L_i and diameter D_i .

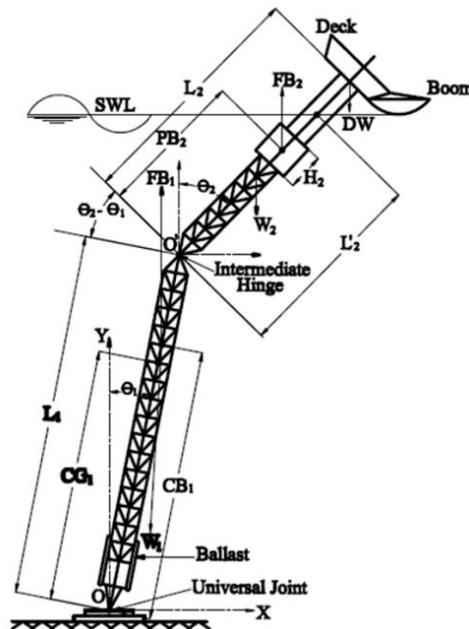


Fig. 2 Mathematical model of double hinged ALP

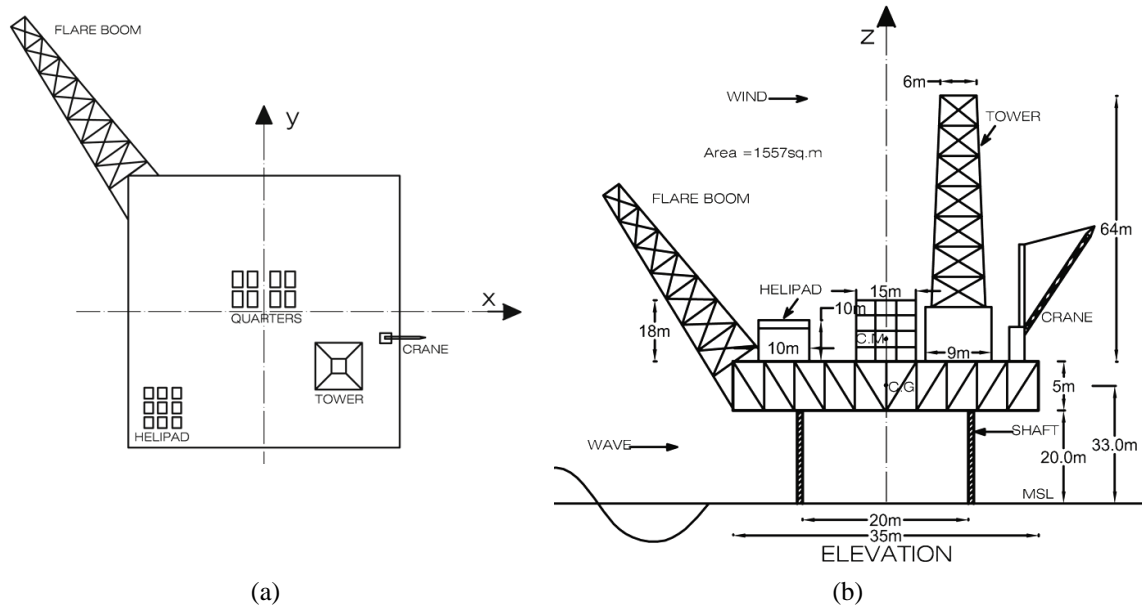


Fig. 3 ALP Configuration (a) Deck plan and (b) Full-scale dimensions of the superstructure

All forces are assumed to act at these centroids and include weight, inertia forces, buoyancy, fluid forces on the submerged parts, and wind forces on the platform above seawater level. Distributed loads on submerged small elements due to the above forces must be transformed to equivalent loads applied at the nodes. The nodal loads are computed by assuming hydrodynamic loading intensity to vary linearly along the element length. The nodal loads are those which, if applied to the elements at the nodes, would produce the same strain energy in the element as the distributed load would when the element nodal degrees-of-freedom are fixed. The wind loads are modeled as described by (Kareem 1983). The analysis due to wind loads is carried out by considering wind velocity as a combination of mean and fluctuating components. Since ALPs are exposed to environmental loading consisting of wind, waves, and current, the influence of wind on ALP cannot be investigated in isolation. Therefore, the model also involves selecting wave theory that reasonably represents the water particle kinematics (velocity and acceleration). Water particle kinematics are calculated at the geometric centroids of each small element and are assumed not to be influenced by the presence of the platform. The error introduced with this assumption is small as long as the ratio of element diameter to wavelength is small. Test calculations have shown that a ratio greater than 0.17 may produce results with an unacceptably large error. Also, to obtain reliable results using Airy's wave theory, ratios of wavelength to wave height should be greater than 10 (Östergaard and Schellin 1987). In the computerized analysis, the equations describing motions and loads of the articulated loading platform are based on Morison's equation applied to a moving system. In order to incorporate a high degree of nonlinearities associated with the system, a time-domain numerical integration scheme is required to solve the equations of motion. The following assumptions have been made while developing the present model:

- The aerodynamic force coefficient of the superstructure is derived using a projected area approach.

- The wind does not modify the wave at mean sea level, and the Airy's linear wave theory is considered valid. The wave diffraction effects have been neglected.
- The total wind force is concentrated at the aerodynamic center (A.C.) of the platform superstructure, while the total mass is acting at its center of gravity (C.G.) of the platform.

2.2 Dynamic analysis

In the following, the dynamic response of a double hinged ALP in surge due to wind and wave excitation is analyzed. The response of the platform is considered based on the application of the two degrees of freedom model, as shown in Fig. 2. Each shaft of the double hinged platform is idealized as a series of 50 elements. The equation of motion (EOM) in structural coordinates takes the form as

$$[M]\{\ddot{x}\} + [C]\{\dot{x}\} + [K]\{x\} = \{F_a + F_d + F_i\} = \{F(t)\} \quad (1)$$

where $[M]$ is the mass matrix consisting of structural mass and added mass; $[C]$ the damping matrix consisting of structural, aerodynamic, and hydrodynamic terms and $[K]$ the displacement-dependent stiffness matrix due to hydrostatic and buoyancy system resistance. The symbol dot represents time differentiation. $\{F(t)\}$ is the forcing function at any instant of time due to waves consisting of drag force F_d , inertia force F_i and due to wind force F_a . Drag and inertia forces are calculated by using Morison's equation. The wind force is calculated by using a sea site wind spectrum. The mass matrix consists of the structural and the added mass portions. The structural mass includes the elemental mass matrices of the bottom and top tower shafts in addition to the deck mass concentrated at the C.G. The structure added mass is arising due to water surrounding the ALP. The variable submergence influence due to the free surface oscillation is modeled using Chakrabarti's stretching modification approach (Chakrabarti 1971). The overall damping is resulting from both the hydrodynamic and structural damping terms. The significant portion of system damping is the hydrodynamic one, which can be obtained from the Morison equation when the term of structural velocity in the forcing function is transferred to the damping term. Rayleigh damping is used in a structural damping simulation.

2.2.1 Mass matrix

The mass matrix, as obtained from (Zaheer and Islam 2012), is diagonal in nature and constant. The presence of off-diagonal terms in the mass matrix indicates added mass contribution due to the hydrodynamic loading. The mass matrix is presented below

$$M = \begin{bmatrix} I_{1t} + \bar{m}_{2t}L_1^2 + m_dL_1^2 & \bar{m}_{2t}L_1c_2 \cos(\theta_2 - \theta_1) \\ \bar{m}_{2t}L_1c_2 \cos(\theta_1 - \theta_1) & I_{2t} + I_d + m_dL_p^2 \end{bmatrix} \quad (2)$$

in which $\bar{m}_{2t} = m_2 + m_a$; m_2 is the mass of the top tower; $m_a = m_{ac} + m_{af}$ is the added mass of the structure, which consists of m_{ac} , the time-invariant added mass upto mean sea level (MSL) and m_{af} , the fluctuating added mass, which depends upon the variable submergence of the structure with respect to MSL with the passage of waves. L_1 is the length of the bottom shaft; I_d is the

moment of inertia of the deck; $L_p = L_2 + P_{cm}$ is the height of C.G. of the deck above mid hinge; L_2 is the length of the top shaft, and P_{cm} is the height of the C.G. above the deck. θ_1 and θ_2 are tilt angles of the bottom and top tower, respectively.

2.2.2 Stiffness matrix

The coefficients of the stiffness matrix of double hinged ALP are derived from the first principles (Zaheer and Islam 2012), is consisting of moment terms of weight and buoyancy. The buoyancy of the system varies at each instant due to the motion of the tower, which makes the stiffness matrix response-dependent. Hence $[K]$ is not constant for each value of time history, but the coefficients are replaced by new values computed at each instant of time depending upon the response value at that time instant. The elements of the stiffness matrix of double hinged ALP are as follows

$$K = \begin{bmatrix} \{(F_1 b_1 - W_1 c_1) + (F_2 - W_2 - W_d) L_1\} \frac{\sin \theta_1}{\theta_1} & 0 \\ 0 & (F_2 b_2 - W_2 c_2 - W_d L_p) \frac{\sin \theta_2}{\theta_2} \end{bmatrix} \quad (3)$$

where F_1 and F_2 are buoyancy forces in the bottom and top tower; W_1 and W_2 are the weights of the lower and upper tower; W_d is the weight of the deck; b_1 and c_1 are the position of the center of buoyancy and center of gravity in the lower tower from the bottom hinge; b_2 and c_2 are the center of buoyancy and center of mass in the upper tower from the mid hinge.

2.2.3 Damping matrix

The structural and hydrodynamic damping is offering the overall damping to the system. The major contribution to the overall damping comes from the hydrodynamic damping. In this study, the structural damping is simulated by Rayleigh damping, which is given by

$$[C] = \alpha[M] + \beta[K] \quad (4)$$

Damping constants, α and β , are the stiffness- and mass-proportional damping constants. These constants are evaluated by selecting the percentage of critical damping (ξ_1 and ξ_2) at the two different natural frequencies (ω_1 and ω_2) of the ALP and solving the following simultaneous equations for α and β (Chopra 2003).

$$\alpha = \frac{2(\xi_2 \omega_2 - \xi_1 \omega_1)}{(\omega_2^2 - \omega_1^2)} \quad (5)$$

$$\beta = \frac{2\omega_1 \omega_2 (\xi_1 \omega_2 - \xi_2 \omega_1)}{(\omega_2^2 - \omega_1^2)} \quad (6)$$

In the present paper, damping constants $\alpha = 0.107$ and $\beta = 0.006$ are determined for a damping ratio of 3% (Jain and Datta, 1990). The set of natural frequencies of the ALP, as they are widely spaced, show that the damping ratios maintain reasonable values for the two modes that are significantly contributing to the ALP response (Chandrasekaran and Nannaware 2014). The damping matrix as obtained by (Zaheer and Islam 2012), takes the form as

$$C = \begin{bmatrix} 0 & -\bar{m}_{2t}L_1c_2\dot{\theta}_2 \sin(\theta_2 - \theta_1)\dot{\theta}_1 \\ \bar{m}_{2t}L_1c_2\dot{\theta}_2 \sin(\theta_2 - \theta_1)\dot{\theta}_1 & 0 \end{bmatrix} \quad (7)$$

2.3 Environmental forces

Three types of forces are considered in the present study, all acting in a direction normal to the tower. The first is for the superstructure portion of the ALP and is due to wind load. This wind-induced force can change the nonlinear response behavior of the double hinged ALP system. Hence, an accurate inclusion of the wind force influence is very important. The second and third are for the submerged part of the tower due to wave and current forces. These forces are elaborated on in the following subsections.

2.3.1 Wind forces

The wind force on the tower is calculated if the wind is expressed as a wind spectrum with a constant direction. The direct wind pressure on the platform superstructure causes motion in surge degree of freedom. As it has been assumed that the total wind force is said to be concentrated at the aerodynamic center (A.C.) while the mass is lumped at the center of gravity (C.G.) of the platform, the difference between them causes additional moments. The basic expression for the wind-induced drag force per unit projected area, normal to the mean wind velocity of the platform, is given by Simiu and Leigh (1984).

$$f_a(y, z, t) = 0.5\rho_a A_p C_p(y, z)[u(z) + u'(y, z, t) - \dot{x}(t)]^2 \quad (8)$$

where $f_a(y, z, t)$ is the force per unit area and is a function of space (y, z) and time (t) ; ρ_a the air density; A_p is the exposed area of the platform in surge direction; $C_p(y, z)$ the pressure coefficient at elevation z and horizontal coordinate y ; $\dot{x}(t)$ the structural velocity in the surge direction; $u(z)$ the mean wind velocity and $u'(y, z, t)$ the fluctuating wind velocity in the surge direction varying with time. In the time-domain analysis, the wind force is directly computed and applied to the tower at each time step.

The wind velocity on the platform is expressed as

$$u(y, z, t) = u(z) + u'(y, z, t) \quad (9)$$

The wind velocity in Eq. (9) has two components, one deterministic $u(z)$ and the other randomly varying with height, $u'(y, z, t)$ above MSL. The deterministic velocity is related to the constant wind speed at 10 m, and the random velocity is related to the mean gust velocity at 10 m. This fluctuating velocity component is estimated by the Fourier synthesis of the wind spectrum suited to the offshore environment (Simiu and Leigh 1984).

The mean wind velocity is a function of height above the sea surface and is represented by logarithmic law as

$$u(z) = u(z_{ref}) \times \ln \frac{z}{z_0} / \ln \frac{10}{z_0} \quad (10)$$

where $u(z_{ref})$ is the reference velocity at 10 m height above the MSL; z the vertical coordinate

above MSL (33.0 m) and z_0 the roughness length, which is approximately 0.005 m for a rough sea surface.

Many types of random wind velocity spectra exist in the published literature. Among them are spectra due to Ochi and Shin, Simiu, Kareem, API RP 2A, Davenport, and others. Low-frequency excitations become very important in the design of ALPs, which can resonate at very low frequencies. Among various models, Ochi and Shin spectrum has higher energy at lower frequencies. It can suitably be applied for offshore applications since it is fitted to measurements over the ocean. Accordingly, Ochi and Shin spectrum (Myrhaug 2007) is chosen to represent the wind with a heading angle of 360 degrees.

$$\begin{aligned} \frac{nS_u(z, n)}{U_*^2} &= 583f_* & 0 < f_* \leq 0.003 \\ \frac{nS_u(z, n)}{U_*^2} &= \frac{420f_*^{0.70}}{(1 + f_*^{0.35})^{11.5}} & 0.003 \leq f_* \leq 0.1 \\ \frac{nS_u(z, n)}{U_*^2} &= \frac{838f_*}{(1 + f_*^{0.35})^{11.5}} & 0.1 \leq f_* \end{aligned} \quad (11)$$

where $f_* = nz/u(z)$ is the dimensionless frequency, and U_* is the friction velocity, and nS_u is the wind velocity spectrum.

The total wind force F_a in surge direction on exposed platform area A_p , is given by

$$F_a(y, z, t) = \int_{A_p} f_a(y, z, t) dydz \quad (12)$$

where A_p is the total projected area of the platform normal to the direction of wind.

2.3.2 Hydrodynamic forces

The hydrodynamic excitations of the offshore articulated loading platforms mainly come from waves and currents. According to the linear theory of waves, ocean waves in deep water conditions can be assumed as a nearly linear superposition of harmonic components. The PSD characterizes standard models of the ocean waves. These models are derived from the observed properties of ocean waves and are thus empirical. The most commonly used spectrum models are Pierson–Moskowitz (P-M) spectrum, Bretschneider spectrum, ISSC spectrum, JONSWAP spectrum, and Ochi-Hubble spectrum (Chakrabarti 2005). In the present study, random waves are represented by the P-M spectrum because of two reasons. Firstly, this model has established applicability for different offshore locations globally. Secondly, the P-M spectrum is a special case of the JONSWAP spectrum, with the peakedness parameter value being one. By considering the random process as a linear superposition of a large number of independent waves, its distribution becomes Gaussian. In the following simulation procedure, waves are assumed to be stationary, homogeneous, and ergodic in the statistical sense. Here, a sea state is represented by the one-sided DNV version of the Pierson-Moskowitz spectrum and is given by

$$S_f = \frac{H_s^2 T_z}{8\pi^2} (T_z f)^{-5} \exp\left[-\frac{1}{\pi} (T_z f)^{-4}\right] \quad (13)$$

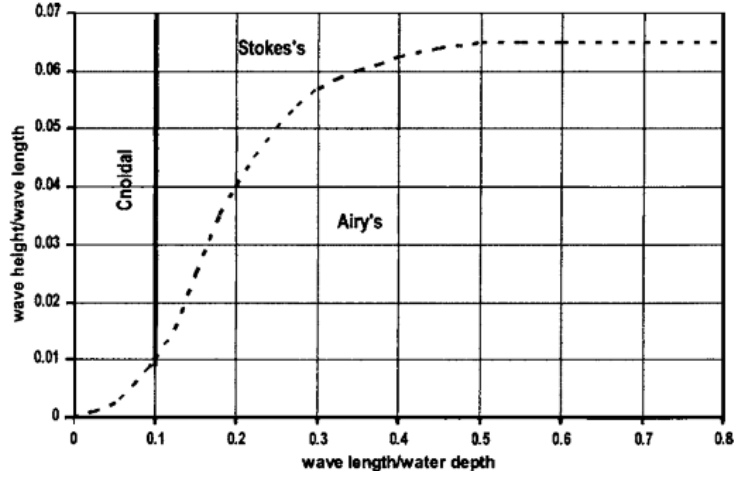


Fig. 4 range of validity of different wave theories (taken from Dawson 1983)

where f is the frequency in cycles per sec; H_s is the significant wave height, which is the average height of the highest one-third of all waves, and T_z is the wave period and S_f is the P-M (single-sided) sea surface elevation spectrum.

It is essential to choose a suitable wave theory for practical considerations of the given water depth d , wave height H , and time period T . The applicability of a particular wave theory may be described by d/λ and H/λ , where λ is the wavelength. Fig. 4 shows the range of acceptability of wave theories based on these two parameters. However, the boundary limits are not fixed in choosing a particular wave theory. The limits of acceptability are based on how well the free surface boundary conditions are satisfied, although there have been limited experimental verifications (Chandrasekaran *et al.* 2007). Although not firmly appropriate to typical design waves used in offshore engineering, the Airy's theory is valuable for preliminary design and for revealing the basic characteristics of wave-induced motion. It also serves as a basis for the statistical representation of waves and induced water motion during harsh sea conditions (Chandrasekaran *et al.* 2007). In many practical conditions, the linear wave theory with stretching modifications as suggested by (Chakrabarti 1971) is inadequate to describe water particle kinematics fully. Therefore, Stoke's fifth order wave theory is vital to achieving better free surface and water particle kinematics. The work on the articulated loading platform (ALP) response using higher-order wave theory is still going on and will be compared and presented in a future paper.

In the present study, water particle kinematics (velocity and accelerations) are evaluated by using Airy's linear wave theory. The horizontal and vertical water particle velocities are

$$\dot{u}_h = \frac{H}{2} \omega \frac{\cosh(k_i z)}{\sinh(k_i d + \eta)} \cos(k_i x - \omega t), \quad \dot{u}_v = \frac{H}{2} \omega \frac{\sinh(k_i z)}{\sinh(k_i d + \eta)} \sin(k_i x - \omega t) \quad (14)$$

and the respective accelerations are

$$\ddot{u}_h = \frac{H}{2} \omega^2 \frac{\cosh(k_i z)}{\sinh(k_i d + \eta)} \sin(k_i x - \omega t), \quad \ddot{u}_v = -\frac{H}{2} \omega^2 \frac{\sinh(k_i z)}{\sinh(k_i d + \eta)} \cos(k_i x - \omega t) \quad (15)$$

where H denotes the wave height; k_i is the i^{th} component wave number ($= 2\pi / \lambda$); wl is the

wave length; ω is the wave frequency ($2\pi / \omega p$); ωp is the wave period; d is the water depth; x is the horizontal distance of the point in the wave travel direction, y is the vertical distance of the point under consideration from the sea bed and η is the free surface profile. The value of η varies from one point to the next on the free surface as a function of x and t , where

$$\eta = \frac{H}{2} \cos(Kx - \omega t) \quad (16)$$

It is noteworthy that wave and current forces naturally occur simultaneously in a real ocean environment. Precise treatment of their combined kinematics is a complex problem. Fortunately, a simple superposition technique is sufficient (Leonard and Young 1985) for most circumstances when the Morison equation is used. An average current velocity of 1.0 m/sec throughout the water depth with a fixed direction is used in the present study. The wave force per unit length of the member of the j^{th} tower at i^{th} location produced due to fluid structure interaction at any instant of time is given by

$$F_h(t) = 0.5\rho_w C_D D_{ji} (\dot{u}_{fi} - r_{ij}\theta_j + v_c) |\dot{u}_{fi} - r_{ij}\theta_j + v_c| + \frac{\pi}{4} C_M \rho_w \pi D_{ji}^2 \ddot{u}_{fi} \pm \frac{\pi}{4} \rho_w D_{ji}^2 (C_M - 1) r_{ij} \ddot{\theta}_j \quad (17)$$

where C_D and C_M are the drag and the inertia coefficients; v_c is the velocity of current; D_{ji} is the diameter of the j^{th} tower for i^{th} element; r_{ij} is the distance of the i^{th} element from the hinge of the j^{th} tower. \dot{u}_{fi} and \ddot{u}_{fi} are the water particle velocity and acceleration normal to the displaced j^{th} tower at i^{th} location; θ_j is the tilt angle of the j^{th} tower and ρ_w is the mass density of seawater. The last term in Eq. (17) is due to the contribution of added mass. The positive sign is used when sea surface elevation, η is below MSL and vice versa.

2.3.3 Correlated wind and waves

In this paper, wind and wave are considered correlated; namely, the wave is assumed to be generated by winds. (Sarpkaya and Isaacson 1981) used the following relationships to describe the significant wave height H_s and wave period T_z , which is correlated with the assumed wind speed at 10 m height. The expected value of the significant wave height and wave period is given by

$$u(z) = \sqrt{\frac{gH_s}{0.283}} \quad (18)$$

$$T_z = \sqrt{\left(\frac{32\pi H_s}{g}\right)} \quad (19)$$

The random wave model will be considered with different wind speeds to study the dynamic response of the ALP under two correlated wind-wave conditions, namely high and moderate sea states. The wind and wave characteristics for the two cases are presented in Table 1. Considering that wind and waves are correlated, the interaction between wind + wave + current constitutes the real ocean environment, and the combined load model may provide more reliable results when compared to the base case of wave + current.

2.3.4 Forcing function

Table 1 Characteristics of sea states

| Wind velocity (m/sec) | Significant wave height H_s (m) | Wave period T_z (sec) | Sea state |
|-----------------------|-----------------------------------|-------------------------|--------------------|
| 25 | 18.0 | 13.6 | High sea state |
| 15 | 6.5 | 8.15 | Moderate sea state |

The forcing function $F(t)$ due to environmental loads acting on the platform is given by

$$F(t) = F_a\{u(z), u', \dot{x}\} + F_d(\dot{u}, v_c, \dot{x}) + F_i(\ddot{x}) \quad (20)$$

in which $F_a\{u(z), u', \dot{x}\}$ = aerodynamic force, $F_d(\dot{u}, v_c, \dot{x})$ = fluid drag force and $F_i(\ddot{x})$ = fluid inertia force.

2.3.5 Simulation of sea states

The simulated waves are generated by means of the wave superposition technique (Goda 1970). The linearized Airy's wave theory allows the summation of velocity potential, wave elevation, and water particle kinematics of discrete waves to form a random wave made up of several components. The generated random wave is considered to be adequately represented by the summation of K number of sinusoidal waves in the random phase. The following relation represents the series representation of sea surface elevation

$$\eta(t) = \sum_{i=1}^K A_i \cos(k_i x - \omega_i t + \phi_i) \quad (21)$$

where

$$A_i = \sqrt{2[S(\omega_i)\Delta\omega_i]} \quad (22)$$

in which, A_i is the amplitude of the i^{th} component wave; k_i is the wavenumber of the i^{th} component wave; ω_i is the wave frequency of the i^{th} component wave; ϕ_i is the phase angle of the i^{th} component wave randomly selected between 0 and 2π , following the normal distribution; K is the number of wave harmonics considered in the simulation; x is the structural displacement; $S(\omega)$ is the PSD value of one-sided sea surface elevation spectrum at the frequency ω_i .

The selection of frequency ω_i is made such that these frequencies are non-correlated so that they do not constitute harmonics with component waves. First, the range of frequencies, from the lowest ω_{\min} to the highest, ω_{\max} is divided into $(k-1)$ sub-ranges with the dividing frequencies comprising a power series of

$$\omega_j' = \omega_{\min} + \frac{\omega_{\max} - \omega_{\min}}{k-1} \quad (23)$$

$$\omega_2' = \omega_1' C_k \quad (24)$$

$$\omega_i' = \omega_{i-1}' C_k \quad (25)$$

$$\omega'_{k-1} = \omega'_1 C_k^{(k-2)} \quad (26)$$

where

$$C_k = \left(\frac{\omega_{\max}}{\omega'_1} \right)^{\frac{1}{k-2}} \quad (27)$$

Then, the secondary dividing frequencies $\omega''_1, \omega''_2, \omega''_3, \dots, \omega''_{k-1}$ are chosen, at random, in respective sub-ranges. The initial frequency ω''_0 is set equal to ω_{\min} , and the last one is set equal to $\omega''_k = \omega_{\max}$. This selection is made with the support of a random-number-generation program on the personal computer. Finally, the component frequency, ω_i and its bandwidth, $\Delta\omega_i$ is calculated by

$$\omega_i = 0.5 (\omega''_{i-1} + \omega''_i) \quad (28)$$

$$\Delta\omega_i = \omega''_i - \omega''_{i-1} \quad i = 1, 2, 3, \dots, k \quad (29)$$

The above procedure of random selection of component frequency is repeated for each run of every single sea surface elevation spectrum. The random phase angle ϕ_i must be chosen such that the resultant function $\eta(t)$ follows the Gaussian distribution. This has been done with the generation of random numbers normally distributed between 0 and 2π . The computation of sea surface elevation by Eq. (21) is done at discrete intervals of time. The time step Δt is set to satisfy the condition given by

$$\Delta t = \frac{2\pi}{5\omega_{\max}} \quad (30)$$

The value Δt is selected as 0.7 second, which is much smaller than the requirement given by Eq. (30). Based on the performed studies, the Gaussian distribution's asymptotic approach is time-consuming for the number of component waves above 50. Hence, the simulation is carried out with 50 component waves. The length of the simulated wave record is controlled so that about 4000 data points are generated in one run.

2.3.6 Solution procedure

Due to the presence of nonlinearities in Eq. (1), it is solved in the time domain by employing a time marching integration procedure. At any time station, j , the iteration starts with an assumed set of values of surge motion, velocity, and acceleration, the same as those of the previous time station. The forcing function $F(t)$, at the j th time station is then determined with the help of the assumed values of surge responses, and initial responses are obtained at the j th time station. $F(t)$ for the next cycle of iteration is computed with the help of these responses, and the new responses are determined as before. The iteration is continued until convergence is achieved. The convergence is attained when the difference between the two consecutive sets of displacement lies within a tolerance limit of 0.1%. The analysis is performed using a P.C. with an i5 processor. The P.C. takes about 22 minutes for the average to converge. For all the response quantities, the tower is initially assumed to be at rest. For various damping present in the system, the transient phase dies out roughly in 5-10

cycles (i.e., for a time of $5T_0 - 15T_0$ sec., where, T_0 is the period of tower vibration in the mode of vibration under consideration). Various time histories recorded for statistical analyses do not contain this transient phase. This is accomplished by considering the incremental form of the equations of motion using the Wilson- θ method. The flow chart presented in Fig. 5 explains the solution procedure by using Wilson- θ method. The time histories of wind loads can be simulated using Fast Fourier Transformation Technique (FFT). In order to satisfy the ergodicity, the duration of simulated time histories is taken as 9 hours, with a sampling interval of 0.7 sec. Time histories were decomposed into Fourier series and simulated using approximately 50 discrete frequencies.

2.3.7 Reliability analysis

Uncertainty may be seen as a measure of the risk of failure of a system. The practice in the past was to design wind-excited structure for equivalent static loads, with uncertainties expressed in the form of safety factors. For assessing the safety and reliability of a structure, uncertainties in the system may be used to calculate the associated probability of failure P_f . The probability of failure is the probability of surpassing performance levels necessary for a particular role. Any complicated structure has more than one mode of failure. In the case of an ALP, failure may be breakage of the articulated joint, large displacements that render the platform inoperational, or unacceptable acceleration levels for human comfort.

Reliability analysis is performed by investigating the limit state function designed to determine conditions leading to a mode of failure. The limit state equation is generally of the form

$$F = R - S \tag{31}$$

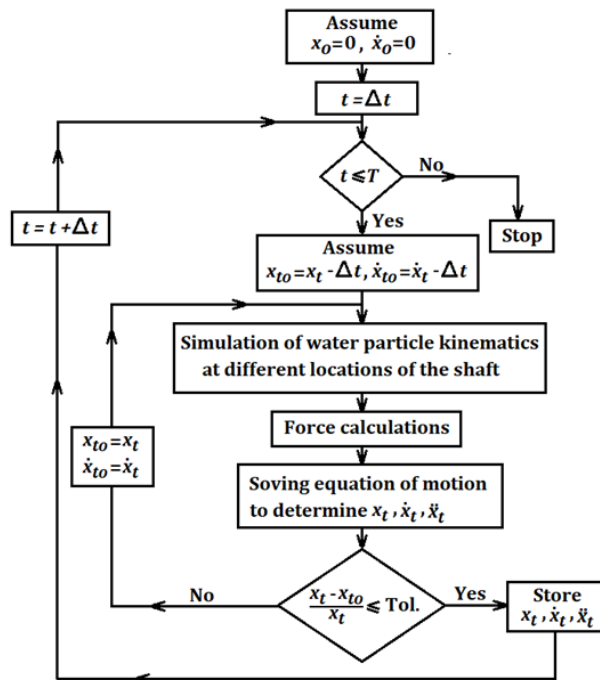


Fig. 5 Flow chart for the method of solution

where failure is indicated by the condition $F < 0$, the resistance R and load S are random variables which may be replaced by the expression necessary in describing the particular mode of failure. Reliability analyses have been carried out using the S-N curve and F-M approaches. A simple reliability analysis is performed for the ALP under consideration using developed software "FATREL" (Fatigue Reliability). The first-order reliability method (FORM) and Monte Carlo simulation methods are systematically employed to find the probability of failure of the articulated joint.

3. Numerical simulation

Numerical studies for evaluating the response of double hinged ALP under different combinations of hydrodynamic and aerodynamics loading has been carried out. The characteristics of sea states are given in Table 1, whereas the ocean environment's characteristics are given in Table 2. The two segments idealized platform with a lumped mass at the top is shown in Fig. 2. The salient properties (weight, buoyancy, deck mass, heights, equivalent diameters, etc.) of the ALP are presented in Table 3. For an adequate discrete representation of the hydrodynamic loading, each shaft of the platform is divided into 50 elements (i.e., $N = 50$) and the number of submerged elements in the undisplaced position of the top tower shaft n_0 is taken as 45. The deck mass above the top shaft is lumped at the C.G of the platform. Plan and superstructure details of the platform deck are shown in Figs. 3(a) and 3(b). For ALP under consideration, the natural frequencies are determined as $\omega_1 = 0.14$ rad/sec in the first mode and $\omega_2 = 0.42$ rad/sec in the second mode using the developed source code DHALP (Double Hinged Articulated Loading Platform). The first mode of the system is that in which both tower shafts are displaced in the same direction and has a much lower frequency and higher amplitude than the second mode, which corresponds to when the tower shafts are displaced in the opposite direction. The code was simulated using FORTRAN Power Station. The flexural rotation of the platform is observed to be of the order of 10^{-7} to 10^{-5} radians, whereas the tilt angle (rigid body rotations) are found to be of the order of 10^{-3} to 10^{-2} radians. Hence, flexural displacements of the tower are neglected in comparison to rigid body displacements. Therefore, the rigid body assumption used for the analysis of these types of platforms is valid. Ochi and Shin wind spectrum is used to plot power spectral density (PSD) of various responses.

Table 2 Characteristics of the ocean environment

| Parameter | units | Value |
|---|-------------------|-----------|
| Drag coefficient of the air | - | 1.81 |
| Mean wind velocity | m/sec | 15 and 25 |
| Air density | Kg/m ³ | 1.27 |
| Reference elevation | m | 33.0 |
| Equivalent area of tower superstructure | m ² | 1557 |
| Mass density of seawater | kg/m ³ | 1025 |
| Coefficient of drag and inertia | - | 0.6, 2.0 |
| Current velocity | m/sec | 1.0 |

Table 3 Principal Characteristics of the tower

| Description | units | Value |
|---|--------------|---------------------|
| Water depth | m | 420 |
| Height of bottom tower | m | 260 |
| Height of top tower | m | 210 |
| Structural mass of top tower | kg/m | 2.0×10^4 |
| Structural mass of bottom tower | kg/m | 2.0×10^4 |
| Mass of ballast | kg/m | 44.84×10^3 |
| Deck mass | kg | 2.5×10^6 |
| Position of buoyancy chamber from the mid hinge | m | 135 |
| Structural frequency (first and second mode) | rad/sec | 0.14 and 0.42 |
| Tower's Shaft | | |
| Effective drag diameter | m | 17.0 |
| Effective diameter for buoyancy | m | 7.5 |
| Effective diameter for inertia | m | 4.5 |
| Effective diameter for added mass | m | 4.5 |
| Buoyancy chamber | | |
| Effective drag diameter | m | 20 |
| Effective diameter for buoyancy | m | 19.5 |
| Effective diameter for inertia | m | 7.5 |
| Effective diameter for added mass | m | 7.5 |

Two sea states are considered corresponding to mean wind velocities of 25 m/sec and 15 m/sec for the analysis. These sea states are designated as high sea state (18.0 m, 13.6 sec) and moderate sea state (6.5 m, 8.15 sec). A constant current profile (1.0 m/sec) through the water depth was assumed where the current velocity is considered in the analysis. The value of drag and inertia coefficients used in Morison's equation are 0.6 and 2.0. Calculations for obtaining time traces are typically carried out over 9 hours, with a time step of 0.7 sec. For simulating the time traces of hydrodynamic loads, 1024 ordinates of the P-M spectrum at random intervals of frequencies were used. Fifty trial simulations of about 22 minutes duration for each random sea state were conducted to get the response statistics. Tower response due to the random sea is influenced by the presence of a combined sea environment. Many interesting qualitative changes are observed by comparing the statistical parameters (maximum, minimum, mean, and standard deviation) and PSDs under various ocean environments.

3.1 Surge response of ALP

3.1.1 Effect of wind on surge response in the presence of wave and current

The large wind-exposed area of the ALP deck attracts wind forces in the surge direction, which caused the dominant motion. The ALP model is subjected to two cases of environmental loading

viz-à-viz random wave of $H_s=18.0$ m, $T_z=13.6$ sec (High sea state) acting along with mean wind velocity of 25 m/sec; the random wave of $H_s= 6.5$ m, $T_z = 8.15$ sec (moderate sea state) acting along with mean wind velocity of 15 m/sec. The results from time-domain analysis with and without wind are presented in Table 4 for high and moderate sea states. As a result of wind force inclusion in addition to random wave and current loads, the platform surge response is directly influenced, and the additional displacement ensued. The maximum surge displacement is 35% and 130% for combined loading cases under high and moderate sea states, respectively. Statistical Table 4 shows that ALP oscillated about a mean value of 10.77 m and 2.70 m, whereas the S.D values are 0.53 m and 0.36 m. Based on the results, it is seen that in the presence of wind, the surge response alters significantly.

Fig. 6 shows the PSD plot under a high sea state. The response spectra are characterized by a significant peak that occurs near the vicinity of the peak frequency of the P-M spectrum. Several peaks are also observed in the low-frequency range showing the influence of wind on the surge response. Fig. 7 presented the PSD plot of the surge response with and without wind for a moderate sea state. The second peak occurs close to the first natural frequency of ALP. The third peak occurs at the platform frequency in the second mode. The first peak appears at a very low-frequency corresponding to the peak frequency of the wind velocity spectrum showing the influence of wind in the surge response. The PSD plot drawn for the wave and current (shown in dotted lines) does not reflect the first peak at the peak frequency of the wind velocity spectrum, and therefore the presence of wind significantly alters the energy content of the surge PSD. Surge response PSD shows a concentration of closely spaced peaks apart from the prominent peaks close to natural frequencies (sometimes higher energy is observed under wave + current). This is because, in time domain analysis, the FFT does not always correspond precisely to the excited frequencies, which are the different modes between any two-wave spectrum components.

3.1.2 Effect of A.C. and C.G. offset on the surge response

By comparing the response given in Table 5 and comparing these values with that obtained with A.C. and C.G. acting collinear, it is seen that there is only a marginal change in the maximum surge response under the two sea states. Based on the above results, it is seen that the location of the aerodynamic center with respect to the center of gravity of the platform does not influence the surge response of ALP significantly.

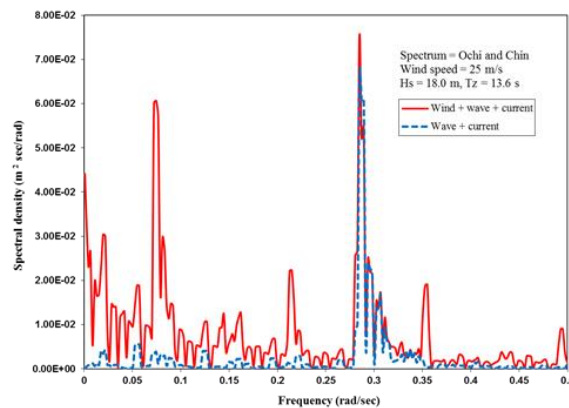


Fig. 6 PSD of surge response under high sea state

Table 4 Surge response of ALP under random ocean environment (m)

| Sea state | Ocean Environment | Maximum | Minimum | Mean | S.D |
|---|-----------------------|---------|---------|-------|------|
| High sea state (18.0 m, 13.6 sec) | wind + wave + current | 12.24 | 9.07 | 10.77 | 0.53 |
| | wave + current | 2.42 | -1.79 | 0.10 | 0.72 |
| Moderate sea state (6.5 m, 8.15 sec) | wind + wave + current | 4.01 | 1.74 | 2.70 | 0.36 |
| | wave + current | 0.28 | -0.08 | 0.22 | 0.05 |

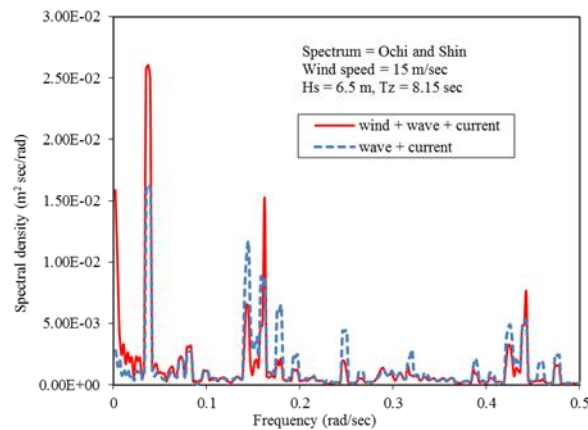


Fig. 7 PSD of surge response under moderate sea state

Table 5 Effect of A.C. and C.G. offset on surge response of ALP under random wind, wave and current (m)

| Ocean Environment | A.C. and C.G. collinear | | | | A.C. and C.G. offset | | | |
|---|-------------------------|------|-------|------|----------------------|------|-------|------|
| | Max. | Min. | Mean | S.D | Max. | Min. | Mean | S.D |
| High sea state (18.0 m, 13.6 sec) | 12.24 | 9.07 | 10.77 | 0.53 | 12.42 | 9.22 | 10.93 | 0.54 |
| Moderate sea state (6.5 m, 8.15 sec) | 4.01 | 1.74 | 2.70 | 0.36 | 4.15 | 2.87 | 3.54 | 0.24 |

3.2 Tilting motion response of ALP

3.2.1 Effect of wind on tilting motion response in the presence of wave and current

The aerodynamic load inclusion increases the upper tilting motion response comparing with the random wave and current case. The top tower shaft rotates in the presence of wind load in addition to the wave and current loads about a mean value of 3.71×10^{-2} rad as presented in Table 6 for high sea state. The statistical Table 6 shows that the maximum and minimum tilting motion values are 4.87×10^{-2} rad and 2.56×10^{-2} rad, respectively. For moderate sea state under the combined wind, wave, and current loads, these values for upper tilting motion were found to be 1.86×10^{-2} rad and 1.34×10^{-3} rad, respectively.

Table 6 Upper tilting motion response of ALP under random ocean environment (rad.)

| Sea state | Ocean Environment | Maximum | Minimum | Mean | S.D |
|---|-----------------------|-----------------------|------------------------|-----------------------|-----------------------|
| High sea state (18.0 m, 13.6 sec) | wind + wave + current | 4.87×10^{-2} | 2.56×10^{-2} | 3.71×10^{-2} | 3.80×10^{-3} |
| | wave + current | 1.72×10^{-2} | -1.51×10^{-2} | 1.62×10^{-4} | 5.71×10^{-3} |
| Moderate sea state (6.5 m, 8.15 sec) | wind + wave + current | 1.86×10^{-2} | 1.34×10^{-3} | 9.01×10^{-3} | 3.01×10^{-3} |
| | wave + current | 2.57×10^{-3} | -2.09×10^{-3} | 2.30×10^{-4} | 3.52×10^{-4} |

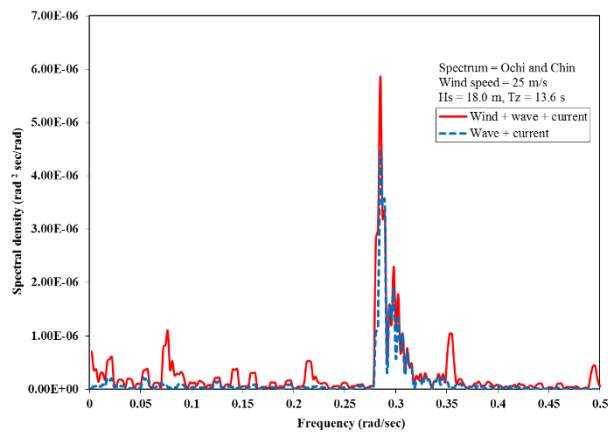


Fig. 8 PSD of upper tilting motion response under high sea state

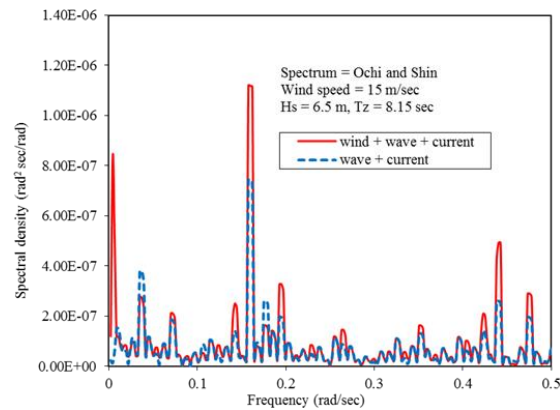


Fig. 9 PSD of upper tilting motion response under moderate sea state

Most importantly, the tilting motion response for both the ocean environments under the two sea states is bounded within 10 degrees from the vertical position of the tower. This indicates that the ALP system is stable to the limit of the parameters and ocean environment tested here (Bithin *et al.* 2015).

Table 7 Effect of A.C. and C.G. offset on upper tilting motion response of ALP under random ocean environment (rad.)

| Sea state | A.C. and C.G. collinear | | | | A.C. and C.G. offset | | | |
|--|-------------------------|----------------------|----------------------|----------------------|----------------------|----------------------|----------------------|----------------------|
| | Max. | Min. | Mean | S.D | Max. | Min. | Mean | S.D |
| High sea state (18.0 m, 13.6 sec) | 4.9×10^{-2} | 2.6×10^{-2} | 3.7×10^{-2} | 3.8×10^{-3} | 4.9×10^{-2} | 2.6×10^{-2} | 3.8×10^{-2} | 3.8×10^{-3} |
| Moderate sea state (6.5m, 8.15 sec) | 1.9×10^{-2} | 1.3×10^{-3} | 9.0×10^{-3} | 3.0×10^{-3} | 1.9×10^{-2} | 8.0×10^{-3} | 1.2×10^{-2} | 1.6×10^{-3} |

Table 8 Central hinge shear response of ALP under random ocean environment (N)

| Sea state | Ocean Environment | Maximum | Minimum | Mean | S.D |
|--------------------------------------|-----------------------|--------------------|---------------------|--------------------|--------------------|
| High sea state (18.0 m, 13.6 sec) | wind + wave + current | 4.37×10^7 | 3.44×10^6 | 2.31×10^7 | 6.72×10^6 |
| | wave + current | 2.51×10^7 | -2.19×10^7 | 2.68×10^5 | 6.08×10^6 |
| Moderate sea state (6.5 m, 8.15 sec) | wind + wave + current | 1.90×10^7 | -6.01×10^6 | 5.79×10^6 | 4.08×10^6 |
| | wave + current | 4.75×10^6 | -3.77×10^6 | 8.95×10^4 | 4.43×10^5 |

The PSD for upper tilting motion response under high sea state is presented in Fig. 8. The response spectra are characterized by a single peak that occurs near the peak energy frequency of the P-M spectrum. Thus, the energy content of the sea spectrum predominantly governs the tilting motion response under high sea state. The peak amplitude at the wave frequency response under wave and current is decreased by about one fourth compared to wave frequency under combined loading.

Fig. 9 shows the PSD plot of the upper tilting motion response under random ocean environment for moderate sea state. The power spectrum displays prominent peaks at the two natural frequencies. The PSD under the combined wind, wave, and current appears to be more energetic than its counterpart due to the extra energy brought by the wind. Further, the PSD plot drawn for the wave and current does not show the first peak at the low-frequency corresponding to the wind velocity spectrum. Therefore, the presence of wind significantly alters the energy content of the tilting motion response.

3.2.2 Effect of A.C. and C.G. offset on the tilting motion response

By comparing the response given in Table 7 and comparing these values with that obtained with A.C. and C.G. acting collinear, it is seen that there is no change in the maximum tilting motion response under the two sea states. On the basis of the above results, it is seen that the location of the aerodynamic center with respect to the center of gravity of the platform does not influence the tilting motion response of ALP.

3.3 Hinge shear response of ALP

3.3.1 Effect of wind on hinge shear response in the presence of wave and current

The central hinge shear response under aerodynamic load along with random wave and current is shown in Table 8. A perceptible increment on the central hinge shear statistical parameters has been observed compared to wave and the current case for both the sea states. The maximum value is increased by 74% in comparison with zero wind effect under high sea state. Whereas, mean and

S.D values of central hinge shear are 2.31×10^7 N and 6.72×10^6 N, respectively. The mean and S.D values under moderate sea state are 5.79×10^6 N and 4.08×10^6 N, Based on the results, it is evident that the presence of wind increases the hinge shear response significantly.

Hinge shear is an important parameter due to stress reversals, which causes fatigue in the articulation points. The response spectra of central hinge shear response under the two ocean environments for high sea state is compared in Fig. 10. The highest peak (0.29 rad/sec) corresponds to the maximum energy content of the sea spectrum. Fig. 11 shows the PSD plot of central hinge shear under moderate sea state. The second and third peak occurs respectively at the two natural frequencies of the platform, but the magnitude of the spectrum is enhanced by about 33% in the presence of wind. The first peak appears at a very low-frequency corresponding to the peak frequency of the wind velocity spectrum showing the influence of wind in the hinge shear response. The PSD plot drawn for the wave and current only (shown by dotted lines) does not reflect the first peak at the low-frequency corresponding to the wind velocity spectrum. Therefore the presence of wind significantly alters the energy content of the central hinge shear. Several smaller peaks in between these dominant frequencies are resulting from the nonlinearity of the system. This nonlinearity may be due to variable submergence, geometric nonlinearity, and forcing function.

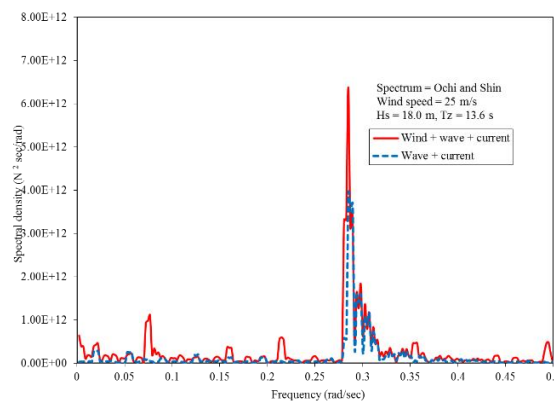


Fig. 10 Comparative time history of central hinge shear under high sea state

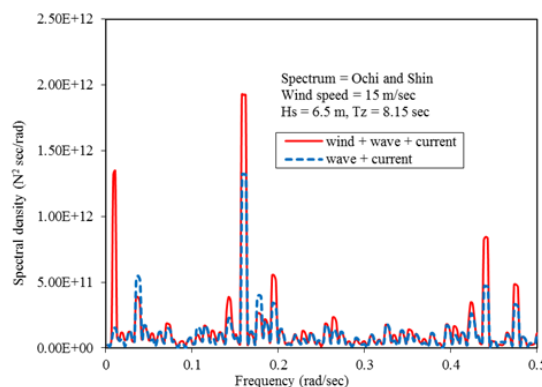


Fig. 11 PSD of central hinge shear response under moderate sea state

Table 9 Effect of A.C. and C.G. offset on central hinge shear response of ALP under random ocean environment (N)

| Ocean Environment | A.C. and C.G. collinear | | | | A.C. and C.G. offset | | | |
|---|-------------------------|---------------------|--------------------|--------------------|----------------------|-------------------|-------------------|-------------------|
| | Max. | Min. | Mean | S.D | Max. | Min. | Mean | S.D |
| High sea state (18.0 m, 13.6 sec) | 4.37×10^7 | 3.44×10^6 | 2.31×10^7 | 6.72×10^6 | 4.4×10^7 | 4.0×10^6 | 2.3×10^7 | 6.6×10^6 |
| Moderate sea state (6.5 m, 8.15 sec) | 1.90×10^7 | -6.01×10^6 | 5.79×10^6 | 4.08×10^6 | 1.4×10^7 | 1.3×10^6 | 7.7×10^6 | 2.8×10^6 |

Table 10 Bending moment response of ALP under random ocean environment (Nm)

| Sea state | Ocean Environment | Maximum | Minimum | Mean | S.D |
|---|-----------------------|-----------------------|------------------------|---------------------|-----------------------|
| High sea state (18.0 m, 13.6 sec) | wind + wave + current | 8.52×10^{10} | -1.01×10^{11} | -5.32×10^9 | 4.63×10^{10} |
| | wave + current | 3.36×10^{10} | -2.11×10^{10} | 1.39×10^8 | 1.21×10^{10} |
| Moderate sea state (6.5 m, 8.15 sec) | wind + wave + current | 3.40×10^{10} | -4.51×10^{10} | -7.71×10^8 | 1.31×10^{10} |
| | wave + current | 3.74×10^9 | -3.11×10^9 | 4.08×10^7 | 6.94×10^8 |

3.3.2 Effect of A.C. and C.G. offset on the hinge shear response

In Table 9, a comparison is made between the hinge shear responses obtained by using A.C. and C.G. collinear and A.C. and C.G. offset. It is seen that A.C. and C.G. offset produce about 2-5% more response in the maximum hinge shear under the two sea states. Based on the above results, it is seen that the location of the aerodynamic center with respect to the center of gravity of the platform influence the hinge shear response to a marginal extent.

3.4 Bending moment response of ALP

3.4.1 Effect of wind on bending moment response in the presence of wave and current

The bending moment response of ALP subjected to the wind load shows noticeable differences comparing with no wind in the random sea environment (Table 10). The mean value shows a significant enhancement in the bending moment response of ALP. The mean value of bending moment is -5.32×10^9 Nm for wind inclusion while the corresponding value for the random wave only is 1.39×10^8 Nm under high sea state. Under moderate sea state, the mean values of bending moment are -7.71×10^8 Nm and 4.08×10^7 Nm, respectively, under the two ocean environments. It is seen from the results that bending moment response is a significant manifestation due to the presence of wind.

The PSD of bending moment under high sea state is shown in Fig. 12. Four peaks characterize the PSD. The fourth peak occurs at the structure's second frequency of the platform. The first peak (also the highest one) occurs at a very low-frequency corresponding to the wind velocity spectrum. The second and third peak occurs, respectively, at structure's first frequency and the wave frequency.

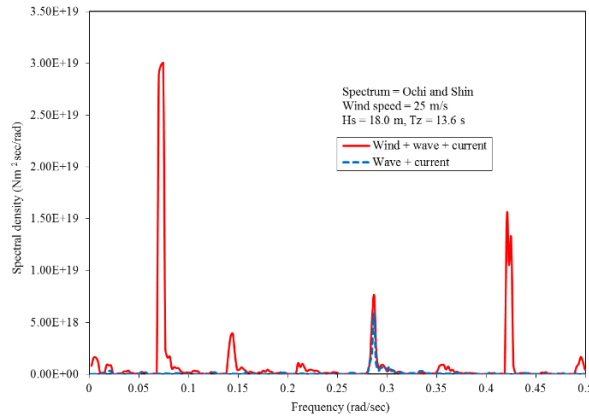


Fig. 12 PSD of bending moment response under high sea state

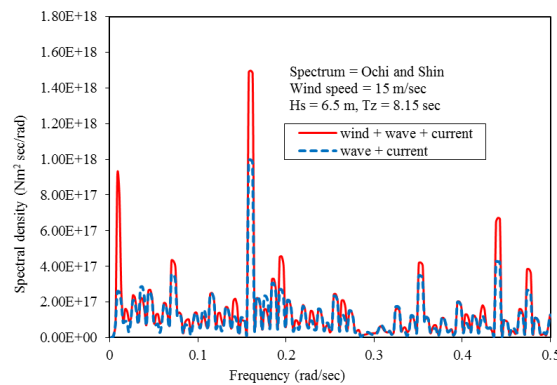


Fig. 13 PSD of bending moment response under moderate sea state

The PSD of bending moment under moderate sea state is characterized by three prominent peaks as shown in Fig. 13. The first peak occurs at a very low frequency, showing the influence of wind on the bending moment response. The third peak occurs at the structure's second fundamental frequency (0.42 rad/sec). The second peak occurs at the structure's first frequency (0.14 rad/sec). The PSD plot drawn for the wave and current only (shown by dotted lines) does not reflect the first peak at the low-frequency corresponding to the wind velocity spectrum, and therefore, the presence of wind significantly alters the energy content of the bending moment response.

3.4.2 Effect of A.C. and C.G. offset on bending moment response

By comparing the response given in Table 11 and comparing these values with that obtained with A.C. and C.G. acting collinear, it is seen that there is a significant increase of 17% in the maximum bending moment response for high sea state. When the A.C. and C.G. become collinear, i.e., the relative coordinates of the A.C. and C.G., along the X-axis is considered to be zero, no additional moments are induced about the Z-axis. Hence, the bending moment response is nominal. However, when A.C. and C.G. become offset, additional moments about the Z-axis results in a substantial increase in bending moment response.

Table 11 Effect of A.C. and C.G. offset on bending moment response of ALP under random ocean environment (Nm)

| Ocean Environment | A.C. and C.G. collinear | | | | A.C. and C.G. offset | | | |
|---|-------------------------|-----------------------|--------------------|----------------------|----------------------|-----------------------|--------------------|----------------------|
| | Max. | Min. | Mean | S.D | Max. | Min. | Mean | S.D |
| High sea state (18.0 m, 13.6 sec) | 8.5×10^{10} | -1.0×10^{11} | -5.3×10^9 | 4.6×10^{10} | 1.0×10^{11} | -1.2×10^{11} | -3.9×10^9 | 4.5×10^{10} |
| Moderate sea state (6.5 m, 8.15 sec) | 3.4×10^{10} | -4.5×10^{10} | -7.7×10^8 | 1.3×10^{10} | 3.0×10^{10} | -3.5×10^{10} | -1.2×10^9 | 1.4×10^{10} |

Table 12 Effect of design life on the probability of failure using the S-N curve approach

| Service life T_L (years) | Wave + current | | Wind + wave + current | |
|----------------------------|------------------------|---------|------------------------|---------|
| | P_f | β | P_f | β |
| 10 | 0.353×10^{-6} | 4.960 | 0.433×10^{-7} | 5.353 |
| 15 | 0.326×10^{-5} | 4.508 | 0.491×10^{-6} | 4.895 |
| 20 | 0.142×10^{-4} | 4.186 | 0.236×10^{-5} | 4.577 |
| 25 | 0.421×10^{-4} | 3.932 | 0.756×10^{-5} | 4.326 |

Table 13 Effect of design life on the probability of failure using the F-M approach

| Service life T_L (years) | Wave + current | | wind + wave + current | |
|----------------------------|------------------------|---------|------------------------|---------|
| | P_f | β | P_f | β |
| 10 | 0.853×10^{-6} | 4.785 | 0.171×10^{-6} | 5.098 |
| 15 | 0.269×10^{-5} | 4.549 | 0.581×10^{-6} | 4.862 |
| 20 | 0.593×10^{-5} | 4.381 | 0.133×10^{-5} | 4.694 |
| 25 | 0.106×10^{-4} | 4.250 | 0.249×10^{-5} | 4.565 |

3.5 Effect of design life

Tables 12 and 13 presents the effect of design life on the probability of failure of the articulated joint under the two loading cases. The probability of failure, P_f steadily increases (or reliability index, β steadily decreases) for an increase in the design life. These outcomes help select the recommended design service life against target reliability. Furthermore, these values are a useful tool for the design of articulated joint as these results are obtained after a comprehensive reliability analysis (Zaheer and Islam 2009). The desired value of the reliability index, as generally recommended for offshore structural components, is 3.0 (Wirsching and Chen 1987). In general, the results of the reliability index of the ALP in Tables 12 and 13 for a design life of 25 years is found to be more than 4.0. These outcomes are helpful for selecting the recommended design service life against target reliability.

4. Conclusions

Dynamic analysis is carried out for double hinged ALP under wind, waves, and current in the time domain. Ochi and Shin wind velocity spectrum and P-M sea surface elevation spectrum are used. The major nonlinearities are incorporated, and their effects on the response are studied using the developed source code DHALP (Double Hinged Articulated Loading Platform). Wind plays a vital role in various platform responses. Power spectral densities (PSDs) gives an idea of the energy content of platform response. Based on the numerical study carried out on the double hinged ALP, the following main conclusions are drawn.

- The aerodynamic surge response of the ALP consists of non-zero mean due to mean wind and the superimposed fluctuating surge response caused by the wind gustiness about the displaced position of the platform. The mean wind modifies the mean position of the surge to the positive side, causing an offset. It oscillates about this offset position under the wind and wave loading.
- The energy content of PSDs for a realistic ocean environment, i.e., wind + wave + current case, is altered considerably as compared to that of wave + current case due to the consideration of correlated wind and waves for the present study. It shows the importance of combined wind, wave, and current interaction in the dynamics of double hinged ALP. The distribution of energy against frequencies for various platform responses provide valuable information used in the design of ALP.
- The hinge shear and bending moment response is a significant manifestation of the wind-induced vibration. It is mainly due to the eccentricity of the aerodynamic center (A.C.) and center of gravity (C.G.) of the platform.
- The geometric properties of the platform, like locations of aerodynamic center (A.C.) and the center of gravity (C.G.), plays a vital role in the overall dynamic response of the platform under the combined loading. The response can be controlled by designing the platform components in such a way to keep the aerodynamic eccentricity resulting from asymmetrical structural geometry in the wind plane to a minimum.
- S-N curve approach yields a significantly conservative estimate of the probability of failure as compared to the F-M approach. The inclusion of mean and fluctuating wind with the random wave and current in the analysis causes a reduction of the probability of failure of the universal joint. This low probability of failure will counter unforeseen wind storms more effectively. These outcomes are helpful for selecting the recommended design service life against target reliability.

References

- Abou-ryan, A.M., Khalil, N.N. and Afify, M.S. (2016), "Dynamic behavior of TLP' s supporting 5 -M.W. wind turbines under multi-directional waves", *Ocean Syst. Eng.*, **6**(2), 203-216.
- Ahmad, S., Islam, N. and Ali, A. (1997), "Wind-induced response of a tension leg platform", *J. Wind Eng. Ind. Aerod.*, **72**, 225-240. [https://doi.org/10.1016/S0167-6105\(97\)00238-9](https://doi.org/10.1016/S0167-6105(97)00238-9).
- Bae, Y.H. and Kim, M.H. (2011), "Discussion on Rotor-floater-mooring coupled dynamic analysis of mono-column-TLP-type FOWT (Floating Offshore Wind Turbine)", *Ocean Syst. Eng.*, **1**(3), 243-248. <https://doi.org/10.12989/ose.2011.1.3.243>.
- Bithin, G., Selvam, R.P. and Sundaravadivelu, R. (2015), "Hydrodynamic Responses of a Single Hinged and Double Hinged Articulated Towers", *Proceedings of the 34th Int. Conference on Ocean, Offshore and Arctic*

- Engineering*, May 31 - June 5, Newfoundland, Canada.
- Chakrabarti, S.K. (1971), "Discussion of Nondeterministic analysis of offshore structures", *J. Eng. Mech. Division*, **97**(3), 1028-1029.
- Chakrabarti, S.K. (2005), *Handbook of Offshore Engineering*. Plainfield, IL: Elsevier.
- Chandrasekaran, S., Jain, A.K. and Chandak, N.R. (2007), "Response behavior of triangular tension leg platforms under regular waves using stokes nonlinear wave theory", *J. Waterw., Port, Coast. Ocean Eng.*, **133**(3), 230-237. [https://doi.org/10.1061/\(ASCE\)0733-950X\(2007\)133:3\(230\)](https://doi.org/10.1061/(ASCE)0733-950X(2007)133:3(230)).
- Chandrasekaran, S., Bhaskar, K., Lino, H. and Brijith, R. (2010), "Dynamic response behaviour of multi-legged articulated tower with and without TMD", *Proceedings of the International Conference on Marine Technology*.
- Chandrasekaran, S., Madhuri, S. and Jain, A.K. (2013), "Aerodynamic response of offshore triceratops", *Ship. Offshore Struct.*, **8**(2), 123-140. <https://doi.org/10.1080/17445302.2012.691271>.
- Chandrasekaran, Srinivasan, and Nannaware, M. (2014), "Response analyses of offshore triceratops to seismic activities", *Ship. Offshore Struct.*, **9**(6), 633-642. <https://doi.org/10.1080/17445302.2013.843816>.
- Chandrasekaran, Srinivasan, and Nassery, J. (2017), "Nonlinear response of stiffened triceratops under impact and non-impact waves", *Ocean Syst. Eng.*, **7**(3), 179-193. <https://doi.org/10.12989/ose.2017.7.3.179>.
- Chopra, A.K. (2003), *Dynamics of Structures*, 5th Ed., Pearson.
- El-gamal, A., Essa, A. and Ismail, A. (2014), "Influence of Tethers Tension Force on the response of Triangular Tension Leg Platform subjected to hydrodynamic waves", *Proceedings of the International Conference on Civil and Architecture Engineering*.
- Goda. (1970), *Numerical experiments on wave statistics with spectral simulation*. Japan.
- Hasan, S.D., Islam, N. and Moin, K. (2011), "Multihinged Articulated Offshore Tower under Vertical Ground Excitation", *J. Struct. Eng. Eng.*, **137**, 469-480. [https://doi.org/10.1061/\(ASCE\)ST.1943-541X.0000284](https://doi.org/10.1061/(ASCE)ST.1943-541X.0000284).
- Islam, A.B.M.S., Jameel, M., Ahmad, S. and Jumaat, Z. (2014), "Structural behaviour of fully coupled spar-mooring system under extreme wave loading", *J. Civil Eng. Management*, **19**, S69-S77. <https://doi.org/10.3846/13923730.2013.801899>.
- Islam, N., Zaheer, M.M. and Ahmed, S. (2009a), "Double hinged articulated tower interaction with wind and waves", *J. Wind Eng. Ind. Aerod.*, **97**(5-6). <https://doi.org/10.1016/j.jweia.2009.07.002>.
- Islam, N., Zaheer, M.M. and Ahmed, S. (2009b), "Response of double hinged articulated tower platforms to wind forces", *Wind Struct.*, **12**(2), 103-120.
- Jain, A.K. and Chandrasekaran, S. (2004), "Aerodynamic behaviour of offshore triangular tension leg platforms", *Proceedings of the ISOPE Conference*, Toulon, France.
- Jain, A.K. and Datta, T.K. (1990), "Nonlinear response of guyed tower to random wave forces", *Probab. Eng. Mech.*, **5**(2), 66-75. [https://doi.org/10.1016/0266-8920\(90\)90009-9](https://doi.org/10.1016/0266-8920(90)90009-9).
- Kareem, A. (1983), "Nonlinear dynamic analysis of compliant offshore platforms subjected to fluctuating wind", *J. Wind Eng. Ind. Aerod.*, **14**(1-3), 345-356. [https://doi.org/10.1016/0167-6105\(83\)90036-3](https://doi.org/10.1016/0167-6105(83)90036-3).
- Kareem, A. (1985), "Wind-Induced Response Analysis of Tension Leg Platforms", *J. Struct. Eng.*, **111**(1), 37-55.
- Karimirad, M. and Moan, T. (2012), "Wave- and Wind-Induced Dynamic Response of a Spar-Type Offshore Wind Turbine", *J. Waterw., Port, Coast. Ocean Eng.*, **138**, 9-20. [https://doi.org/10.1061/\(ASCE\)WW.1943-5460](https://doi.org/10.1061/(ASCE)WW.1943-5460)
- Kim, H.C. and Kim, M.H. (2015), "Global performances of a semi-submersible 5MW wind-turbine including second-order wave-diffraction effects", *Ocean Syst. Eng.*, **5**(3), 139-160. <https://doi.org/10.12989/ose.2015.5.3.139>.
- Leonard, J.W. and Young, R.A. (1985), "Coupled response of compliant offshore platforms", *Eng. Struct.*, **7**(2), 74-84. [https://doi.org/10.1016/0141-0296\(85\)90017-3](https://doi.org/10.1016/0141-0296(85)90017-3).
- Malayjerdi, E. and Tabeshpour, M.R. (2016), "Frequency domain analysis of Froude-Krylov and diffraction forces on TLP", *Ocean Syst. Eng.*, **6**(3), 233-244. <https://doi.org/10.12989/ose.2016.6.3.233>.
- Moharrami, M. and Tootkaboni, M. (2014), "Reducing response of offshore platforms to wave loads using hydrodynamic buoyant mass dampers", *Eng. Struct.*, **81**, 162-174. <https://doi.org/10.1016/j.engstruct.2014.09.037>.

- Myrhaug, D. (2007), "Wind gust spectrum over waves: Effect of wave age", *Ocean Eng.*, **34**, 353-358. <https://doi.org/10.1016/j.oceaneng.2006.01.003>
- Nagavinothini, R. and Chandrasekaran, S. (2019), "Dynamic analyses of off shore triceratops in ultra-deep waters under wind, wave, and current", *Structures*, **20**, 279-289. <https://doi.org/10.1016/j.istruc.2019.04.009>.
- Östergaard, C. and Schellin, T.E. (1987), "Comparison of experimental and theoretical wave actions on floating and compliant offshore structures", *Appl. Ocean Res.*, **9**(4), 192-213. [https://doi.org/10.1016/0141-1187\(87\)90002-2](https://doi.org/10.1016/0141-1187(87)90002-2).
- Oyejobi, D.O., Jameel, M., Hafizah, N. and Sulong, R. (2016), "Stochastic Response of Intact and a Removed Tendon Tension Leg Platform to Random Wave and Current Forces", *Arab J. Sci. Eng.*, <https://doi.org/10.1007/s13369-016-2282-4>.
- Philip, V., Joseph, A. and Joy, C.M. (2015), "Three Legged Articulated Support for 5 MW Offshore Wind Turbine", *Aquatic Procedia*, 4(Icwrcoe), 500-507. <https://doi.org/10.1016/j.aapro.2015.02.065>.
- Rahman, M., Islam, A.B.M.S., Zamin, M. and Huda, N. (2017), "Response of nonlinear offshore spar platform under wave and current", *Ocean Eng.*, **144**, 296-304. <https://doi.org/10.1016/j.oceaneng.2017.07.042>.
- Saiful Islam, A.B.M. (2018), "Dynamic characteristics and fatigue damage prediction of FRP strengthened marine riser", *Ocean Syst. Eng.*, **8**(1), 21-32. <https://doi.org/10.12989/ose.2018.8.1.021>.
- Santo, H., Taylor, P.H., Bai, W. and Choo, Y.S. (2015), "Current blockage in a numerical wave tank : 3D simulations of regular waves and current through a porous tower", *Comput. Fluid.*, **115**, 256-269. <https://doi.org/10.1016/j.compfluid.2015.04.005>
- Simiu, E. and Stefan D.L. (1984), "Turbulent Wind and Tension Leg Platform Surge", *J. Struct. Eng.- ASCE*, **110**(4), 785-802.
- Sarpkaya, M. and Isasson, T. (1981), *Mechanics of wave forces on offshore structures*, 1st Ed. the University of California: Van Nostrand Reinhold Co.
- Wirsching, P.H. and Chen, Y.N. (1987), "Fatigue design criteria for TLP tendons", *J. Struct. Eng.- ASCE*, **113** (7), 1398-1414.
- Ye, K. and Ji, J. (2019), "Current , wave , wind and interaction induced dynamic response of a 5 MW spar-type offshore direct-drive wind turbine", *Eng. Struct.*, **178**, 395-409. <https://doi.org/10.1016/j.engstruct.2018.10.023>.
- Zaheer, M.M. and Islam, N. (2008), "Aerodynamic response of articulated towers: state-of-the-art", *Wind Struct.*, **11**(2), 97-120.
- Zaheer, M.M. and Islam, N. (2009), "Fatigue and fracture reliability of articulated tower joint under random loading", *Proceedings of the 28th Int. Conf on Ocean, Offshore and Arctic Engineering*, Honolulu, Hawaii, USA, May 31-June 5, doi:10.1115/OMAE2009-79360.
- Zaheer, M.M. and Islam, N. (2010), "Reliability analysis of universal joint of a compliant platform", *Fatigue Fract. Eng. Mater. Struct.*, **33**(7), 408-419. <https://doi.org/10.1111/j.1460-2695.2010.01453.x>.
- Zaheer, M.M. and Islam, N. (2012), "Stochastic response of a double hinged articulated leg platform under wind and waves", *J. Wind Eng. Ind. Aerod.*, **111**, 53-60. <https://doi.org/10.1016/j.jweia.2012.08.005>.
- Zaheer, M.M. and Islam, N. (2017), "Dynamic response of articulated towers under correlated wind and waves", *Ocean Eng.*, **132**, 114-125. <https://doi.org/10.1016/j.oceaneng.2017.01.019>